4. Reaction dynamics of fs-laser induced associative CO desorption

This chapter provides the results concerning the mechanism of the fs-laser induced associative desorption of CO from Ru(001) covered with ***atomic*** *O and C. A first section gives an overview over the adsorbate system O/C/Ru(001) and its likeliness regarding non-adiabatic adsorbate-substrate interactions. Afterwards the experimental data are presented and the outcome of its modeling within a frictional approach is given. An extensive discussion reveals the reaction mechanism. The energy transfer into the translational degree of freedom of the desorbing CO particle flux is interpreted taking into account the peculiarities of the potential energy surface governing the recombination.*

4.1. The adsorbate system O/C/Ru(001)

In contrast to the almost nonactivated desorption of hydrogen from Ru(001), the recombinative desorption of CO from the same surface exhibits a high barrier. Therefore, CO can be considered as a "model system" for studying activated associative desorption. In the following, the adiabaticity of this type of surface reactions will be discussed and the adsorbate system O/C/Ru(001) will be characterized.

4.1.1. Non-adiabatic effects

The similar potential energy surface (PES) topologies for the activated dissociation of π-bonded molecules on d-band transition metals [Mav99, Ham00b] suggest to discuss the associative desorption of CO from Ru(001) with respect to the well-studied recombinative desorption and dissociative adsorption of N_2 from resp. on Ru(001) [Die00b, Die01, Die02, Lun05, Día06a, Día06b]. Figure 4.1(a) shows the PES for N_2/Ru(001) system. The barrier towards associative desorption is mainly along the vibrational coordinate d and found to be $\approx 2\,\mathrm{eV}$ [Die00b]. The PES exhibits a very shallow metastable chemisorption well for N_2 bonded parallel to the surface [Mur99].

Diekhöner et al. report experiments where simultaneously the rovibrational and translational energy of the associative desorption flux of N_2 from Ru(0001) are determined [Die00b, Die02]. The experiments show that the nascent N_2 is formed with little vibrational excitation, which is not expected for an activated adiabatic process with a barrier along the vibrational coordinate d (see Section 1.1.2). The total excess energy in all N_2 degrees of freedom accounts for only 1/3 of the transition barrier energy. Thus, roughly 2/3 of the energy necessary to surmount the barrier is lost to the surface during desorption. This energy loss could not be attributed to the coupling to the ruthenium lattice and thus, non-adiabatic coupling to the substrate

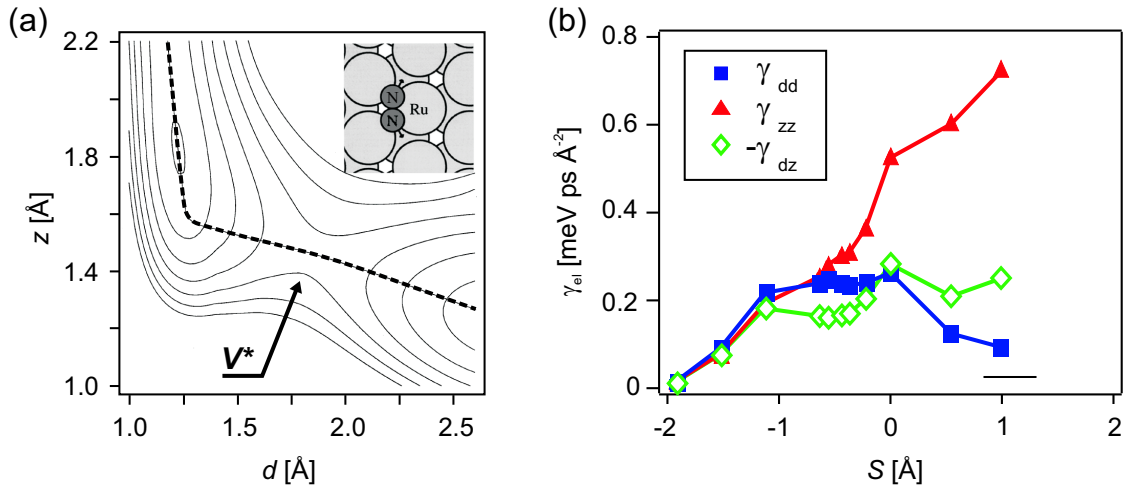

Figure 4.1.: Associative desorption of N_2 from Ru(001). (a) 2D cut of the potential energy surface. d and z denote the intramolecular distance and the center-of-mass to surface distance, respectively. The N_2 lies parallel to the surface, in the geometry indicated in the inset. The dotted line indicates the minimum reaction path S. Figure taken from [Mur99]. (b) *Ab initio* friction coefficients along the minimum energy reaction path S. $S = 0$ is the location of the barrier V^*. Positive S denote atomically bound adsorbates, whereas negative S denote transition to the molecularly bound adsorbate. The solid line at $S = 1$ represents the friction coefficients γ_{zz} for atomic hydrogen adsorbed on Ru(001) (see Section 3.4). Data taken with courtesy of A.C. Luntz from [Lun05].

electrons was suggested [Die02]. Recently, Luntz et al. [Lun05] calculated *ab initio* electronic friction coefficients for the N_2/Ru(001) system and showed that the non-adiabatic effects are quite important during this surface reaction[1]. The calculated friction coefficients γ_{el} along the two dimensional minimum energy reaction path S are depicted in Fig. 4.1(b). The friction coefficients γ_{el} are approximately one order of magnitude larger than these for the hot electron mediated associative desorption of H_2 from Ru(001), which has been discussed in Section 3.4 [Lun05, Lun06]. This and the similarities between the N_2/Ru(001) and CO/Ru(001) system suggest that non-adiabatic effects should be also observable in the femtosecond laser induced associative desorption of CO from Ru(001).

In addition, the investigation of the associative desorption of CO instead of N_2 offers the possibility of probing the internal CO stretch vibration during the surface reaction, since CO exhibits in contrast to N_2 a large dipole moment required for vibrational spectroscopy via sum-frequency generation (SFG) (see Section 2.4.4). This means one can try to detect molecular CO stretch vibration at the transition state or before it leaves the surface and could thus gain direct insight into the reaction kinetics.

4.1.2. Current research status: O/C/Ru(001)

The adsorbate system O/C/Ru(001) is prepared as described in detail in Section 2.5.2. Atomic carbon is obtained from ethylene decomposition [Hrb85, Liv00] and atomic oxygen from nonactivated O_2 dissociation [Ove98]. The atomically bound carbon adsorbs on the threefold hcp hollow site [Mav98] as well as atomically bound oxygen does [Sta96, Ove98]. On the

[1] An outline of the applied theoretical concept is given in Appendix A.

clean ruthenium surface, the binding energy per carbon atom is 6.3 eV [Wis83], whereas oxygen is bound with an energy of 4.9 eV per atom [Sta96, Ove98]. The PES governing the CO recombination on Ru(001) should be similar to the one depicted for the system N_2/Ru(001) in Fig. 4.1(a) [Mav99, Ham00b]. The barrier towards CO *recombination* is located mainly along the vibrational coordinate [Mav98] and calculated to be 1.8 eV [And05], whereas the barrier height for CO *dissociation* is 1.0 eV [Mav98][2]. Thus, the energy required to overcome the barrier is depending along which direction the transition state is traversed. The higher energy for recombination is due to the very strong binding of the atomic adsorbates to the Ru(001) substrate.

In addition to atomically bound C and O, CO can also adsorb molecularly on Ru(001) and (2×1)O/Ru(001), respectively. The latter is present in the performed experiments, since the O/C/Ru(001) preparation procedure involves saturation of the Ru(001) surface with oxygen (see Section 2.5.2). In contrast to N_2/Ru(001), where molecular N_2 is only weakly bound in a metastable state with its molecule axis parallel to the surface, the CO molecule is strongly bound in an upright linear fashion through the C atom to a single Ru atom [Kos92]. The binding energy depends on the CO coverage and two main states with binding energies of 0.5 and 0.9 eV have been identified [Hof91, Kos92].

In principle, the associative desorption of O_2 from O/C/Ru(001) represents a competing reaction channel to the CO recombination. The barrier towards desorption is experimentally determined to be 3.5 eV [Mad75] and thus almost twice as large as the one for CO recombination. This seems surprising since atomic oxygen is less strongly bound than atomic carbon as discussed above. It is the release of the dissociation energy of 11.1 eV for molecular CO twice as large compared to O_2 [Atk87] which makes the CO recombination energetically the much more favorable reaction. Thus, O_2 recombination can be excluded as a competing desorption process in the present case.

4.1.3. Thermal desorption spectroscopy

The different CO binding sites can be probed via by TDS. Discrimination between the molecularly and dissociatively adsorbed species is unambiguously possible by using isotopically labeled reactants. Figure 4.2 shows a TDS of a saturated CO layer on an oxygen saturated O/C/Ru(001) surface. Desorption of the molecularly bound species occurs in the temperature range from 150 to 400 K. Two main features, denoted γ_1 and γ_2, correspond to the two binding states mentioned above. The pronounced shape of these desorption features corroborates the assumption of an almost undisturbed (2×1)O/Ru(001) surface without major changes due to the small amount of absorbed carbon [Kos92].

Associative CO desorption occurs at temperatures ranging from 450 to 750 K. The shape of the TD spectrum is typical for a C/Ru(001) preparation procedure based on the decomposition of C_2H_4 [Lau86, Lau87]. The associative thermal desorption of CO is investigated as a function of the carbon pre-coverage θ_C. Coverages of different θ_C are obtained by dosing a varying amount of ethylene during the preparation. θ_C is denoted in terms of monolayer (ML), with

[2]This DFT calculation used the PW91 exchange correlation functional. It has to be noted that the barrier heights calculated by DFT depend on the applied exchange correlation functional and a lower barrier height might be expected from applying the PW91 instead of the RPBE approximation [Die01]. The latter was used to calculate the barrier of 1.8 eV for CO recombination.

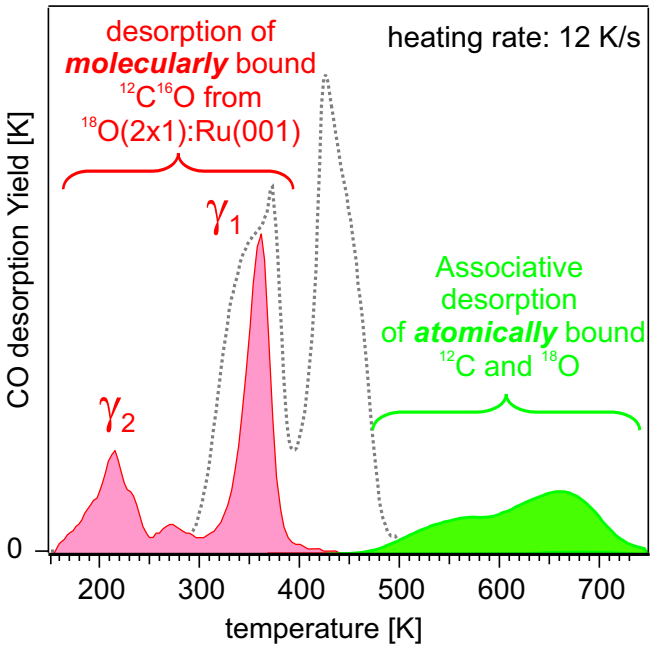

Figure 4.2.: TDS of a saturated $C^{16}O$ layer from a pre-covered $(2\times1)^{18}O/C/Ru(001)$ surface. The molecular adsorbed $C^{16}O$ desorbs at distinct lower temperatures ranging from 150 to 400 K than the associatively formed $C^{18}O$ desorbing at temperatures higher than 450 K. For comparison a TDS of a saturated CO layer on Ru(001) is depicted by the dashed line.

1 ML corresponding to a ratio of one between carbon and ruthenium surface atoms. The thermal desorption[3] spectra for varying θ_C are depicted in Fig. 4.3. The applied heating rate is $\beta = 12\,K/s$. Carbon coverages range from 0.003 to 0.14 ML. A second oxidation cycle not shown and not showing any CO desorption assures that also at high θ_C all surface carbon oxidizes and desorbs during the first heating of the crystal. From investigations concerning the adsorption of O_2 on carbon-covered Ru(001), it is known that the maximum amount of adsorbed atomic oxygen decreases with increasing θ_C [Shi80a]. In our case $\theta_{C,max} = 0.14\,ML$ a maximal ratio of $\theta_C/\theta_O = 1/3$ is obtained, decreasing to 1/10 for $\theta_C = 0.04$, where all the fs-laser induced desorption experiments are performed.

The TD spectra show a pronounced structure composed of a low and high temperature feature denoted as LT and HT peak, respectively. As can be seen from Fig. 4.3(b), the data is very well reproduced by fitting the sum of two Gaussian distributions. The inset of Fig. 4.3(a) shows the integrated area of the two Gaussian distributions as a function of θ_C. An increase of θ_C up to 0.08 ML leads to an almost equal increase of the contributions, whereas mainly the HT peak benefits from carbon pre-coverages higher than $\theta_C = 0.08\,ML$.

The vertical lines in Fig. 4.3(b) indicate the dependence of the peak temperatures T_{max} on θ_C. The LT peak maximum is constant at $T_{max,LT} \approx 560\,K$, whereas $T_{max,HT}$ shifts with increasing θ_C from ≈ 610 to $\approx 670\,K$. The constant peak temperature observed for the LT-feature indicates a first order reaction mechanism [Chr91]. On the other hand, associative desorption is generally expected to be a second-order reaction [Men75, Chr91]. In the present case of the low θ_C/θ_O ratios specified above, the two reactants are no longer equal with respect

[3] In the following, thermal desorption (TD) of CO and thermal oxidation of carbon followed by subsequent CO desorption will be used synonymously.

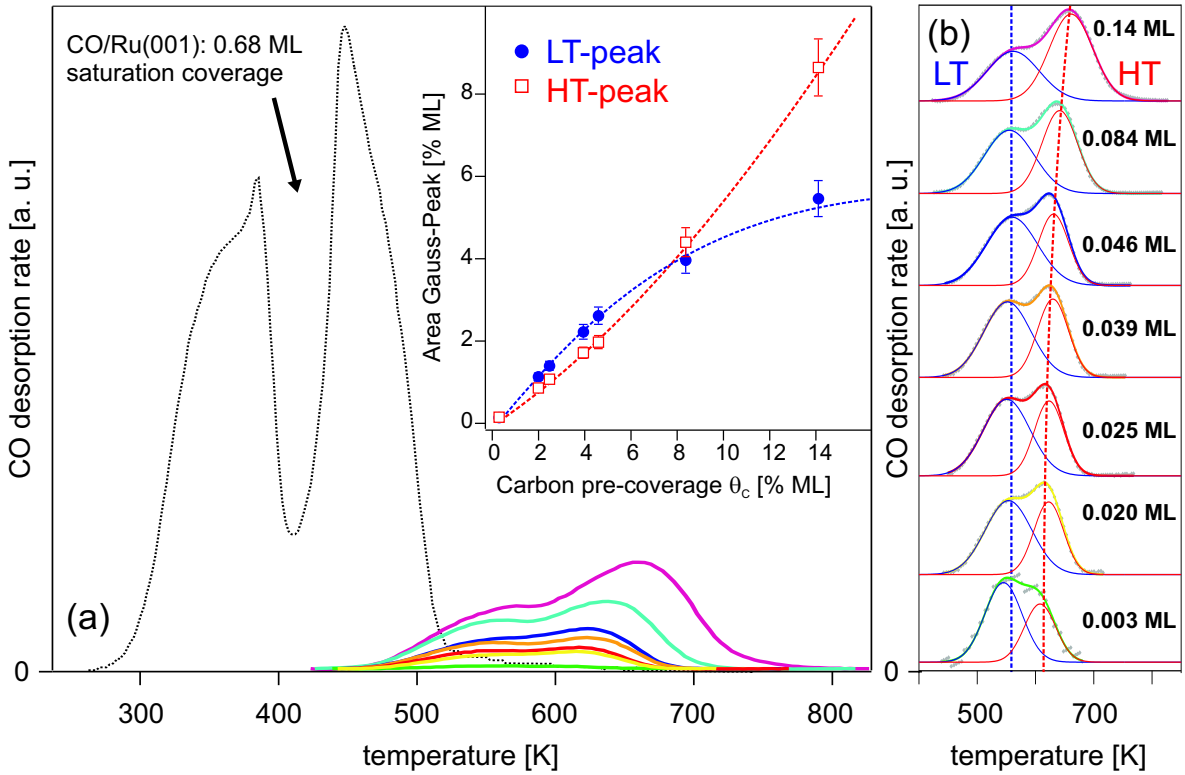

Figure 4.3.: (a) Thermal desorption spectra (heating rate $\beta = 12\,\mathrm{K/s}$) of associatively desorbing CO from Ru(001) as a function of carbon pre-coverage θ_C. The coverages are denoted in (b), where in addition fits to the TD spectra are shown. The sum of two Gaussian distribution reproduces very well the two-peak structure of the data. The individual Gaussians are plotted and vertical lines indicate the dependence of the two peak temperatures on θ_C. The inset of (a) shows the increase of the two contributions with increasing θ_C. LT and HT stand for low and high temperature, respectively, and the dashed lines are guides to eyes. (For comparison, a TD spectra of CO desorbing from the molecular state from a saturated Ru(001) surface is shown as a dashed line in the left panel.)

to their contribution to the reaction rate. Since there is always a filled oxygen "reservoir", merely the carbon concentration is rate-limiting, which makes the reaction pseudo first order. Thus, the activation energy E_a can be obtained as a function of the pre-exponential fastor ν via [Red62]

$$E_\mathrm{a} = k_\mathrm{B} T_\mathrm{max} \left(\ln \frac{\nu T_\mathrm{max}}{\beta} - 3.46 \right), \tag{4.1}$$

which is only valid for first order desorption. Equation (4.1) implies that E_a is only unambiguously determinable if ν is known. For "normal" prefactors of $\nu{\sim}10^{12} - 10^{13}\,\mathrm{s}^{-1}$ (see Section 1.3.2) and the experimental parameters ($T_\mathrm{max} = 560\,\mathrm{K}$; heat rate $\beta = 12\,\mathrm{K/s}$), E_a results in 1.5(1) eV, which is in reasonable agreement with the DFT value of 1.8 eV [And05].

No effort is undertaken to determine the activation energy of the HT desorption feature, which is most likely not unambiguously possible due to the overlapping peak structure [Daw72, Pis74, Men75]. As will be seen in Section 4.2.1, the adsorbed carbon species responsible for the HT peak does not contribute to the fs-laser induced reaction rate. Thus, the parameters governing the HT desorption process are not required for the interpretation of the experimental results obtained for the fs-laser induced CO recombination.

The microscopic origin of the two peak structure is thought to be as follows: the LT feature is assigned to recombination of *reactive* carbon and oxygen on adjacent sites, whereas the second order-like behavior of the HT peak is suggested to be due to the onset of surface mobility of less reactive adsorbates at $\approx 650\,\mathrm{K}$ giving rise to a surface diffusion controlled reaction [Lau86]. Since a hopping rate of 10^5 s^{-1} at 400 K is found for atomic oxygen on Ru(001) [Ham00a], it is very likely that the surface mobility of the more strongly bound carbon species is the rate-limiting step governing the TDS HT feature. This assumption is corroborated by experiments performed by Diekhöner et al. [Die01, Die00a], who prepared atomically bound C on Ru(001) via the dissociation of methane. This preparation procedure assures that initially isolated carbon atoms are formed, which can be oxidized to CO and desorb at $\approx 570\,\mathrm{K}$. After annealing of a carbon pre-covered Ru(001) surface up to 660 K, the formation of a high-temperature TDS feature desorbing at a peak temperature of $\approx 700\,\mathrm{K}$ is observed [Die01]. This means that due to surface mobility of carbon a more strongly bound so-named C_2 structure is formed, which might be initially present applying a C/Ru(001)-preparation procedure based on ethylene decomposition.

4.1.4. Dissociation and recombination at steps

It is well known that the surface reactivity concerning the dissociation of π-bonded molecules on transition metal surfaces can be greatly enhanced by few highly reactive sites, most-likely steps [Zam96, Dah99, Dah00b]. Thus one has to assure that the investigated associative desorption of CO (as the reverse process of dissociation) is not dominated by recombination at steps. Zubkov and co-workers investigated the dissociation of CO on stepped Ru(109) surface, which exhibits, due to reconstruction, a step density of 10% [Zub02, Zub03]. A significant amount of dissociated CO is obtained and desorbs recombinatively at $\approx 520\,\mathrm{K}$. The step density of the Ru(001) surface used in the present experiments is experimentally determined via a CO titration procedure according to [Shi85] and a conservative upper bound of 1% step density is obtained. The following arguments allow to neglect recombination at steps for the present investigation: As discussed above, the surface mobility of carbon is very low at $T = 520\,\mathrm{K}$, where the recombination at steps occur and the measured thermal CO desorption rate is larger than 1% of a monolayer. Thus it can not be contributed to the steps. Furthermore, the desorption occurs at significantly higher temperatures than observed for dissociation at steps. The strongest argument results from the consideration of the short timescales on which a fs-laser induced reaction takes place. Since the surface cools down to its initial temperature within $\sim$10 ps, diffusion of the reactants can be neglected. As will be seen in Section 4.2.1, the observed reaction yields for fs-laser induced CO recombination can not be explained with a surface concentration of the reactants as small as the upper limit of 1% for the step density. This is contradictory to a recombination scenario at step sites. Thus, the data presented in Section 4.2 can be unambiguously related to CO recombination on Ru(001) terrace sites.

4.2. Experimental results

In the following, the experimental results obtained for the fs-laser induced associative desorption of CO from a O/C/Ru(001) surface will be presented. The reaction yield was investigated concerning its dependence on carbon coverage (Section 4.2.1), fluence and wavelength (Section 4.2.2), wherefrom the reaction cross section is determined (Section 4.2.2). The outcome of two-pulse correlation (2PC) measurements (Section 4.2.3) and the influence of isotopically marked reactants are investigated as well (Section 4.2.4). The energy transfer to the translational degree of freedom of the desorbing CO molecules is determined and shown in Section 4.2.5. The modeling of the experimental data within the framework of a friction approach is given in Section 4.3 and will be discussed in detail in Section 4.4.

All experiments have been performed with an initial surface temperature $T_S = 400\,K$, which assures that no molecular CO is adsorbed on the surface and that the detected CO originates from associative desorption. Except the investigation of the coverage dependence, all fs-laser induced desorption experiments have been performed with carbon pre-coverages $\theta_C \approx 0.04$ ML. All laser fluences $\langle F \rangle$ are yield-weighted fluences (YWF) taking into account a possible nonlinear behavior of the reaction rate on the laser fluence and all reaction yields are first-shot yields (FSY). Detailed definitions of the YWF and the FSY are given in Section 2.5.

4.2.1. Coverage dependence

The fs-laser induced associative desorption of CO from Ru(001) is investigated as a function of the carbon coverage θ_C for two fluences of the 800 nm fs-laser pulse, namely $\langle F \rangle = 140$ and $190\,\mathrm{J/m^2}$. The first shot yield as a function of θ_C is depicted in Fig. 4.4(a). The observed behavior is the same for both fluences, whereas an approximately twice as large yield is obtained for the higher fluence. As can be seen, the yield increases with θ_C, whereby a strong weakening of the increase is observed for $\theta_C > 0.05$ ML. This means that the additional carbon adsorbates for $\theta_C > 0.05$ ML do not heavily contribute to the measured desorption rate. This behavior resembles the increase of the low temperature (LT) TDS feature with θ_C depicted in the inset of Fig. 4.3(a). The LT-TDS feature, which results from oxidation of "highly reactive" isolated carbon atoms, exhibits a saturation of the increase with increasing θ_C as well as the fs-laser induced reaction yield. Therefore, the laser induced desorption yield is plotted against the area of the LT TDS feature in Fig. 4.4(b). A proportionality depicted by the dotted lines reproduces well the experimental findings. Small deviations, especially at low coverages, most likely arise from the difficulty of determining the correct ratio between the LT and HT TDS features in the case of an overlapping TD spectrum. The applied Gaussian distributions are well suited to determine peak temperatures, whereas they do not reproduce the exact TD shape for a first order desorption process [Men75, Chr91].

In summary, it can be stated that the yield of the fs-laser induced associative desorption of CO from O/C/Ru(001) does mainly results from an adsorbed atomic carbon species responsible for the LT peak in the TD spectra. As discussed in Section 4.1.3, this species can be characterized as being isolated "highly" reactive carbon atoms. Thus, one can restrict the discussion of the fs-laser driven CO recombination to the case of isolated adsorbates and ignore possible influences of neighboring C-C atoms being responsible for the HT TDS feature.

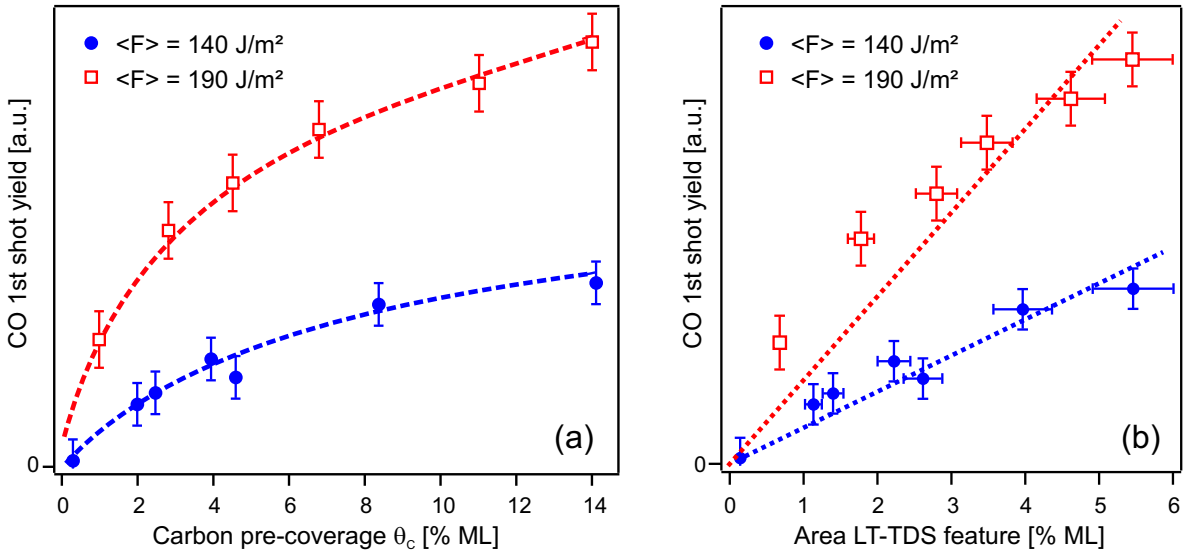

Figure 4.4.: (a) Dependence of the fs-laser induced associative CO desorption yield on carbon coverage θ_C. The depicted data sets are obtained from 800 nm excitation with yield-weighted fluences of 140 and 190 J/m^2, respectively. Dashed lines are guide to the eye.(b) Plot of the FSY against the area of the LT-TDS feature for various coverages θ_C (see Fig. 4.3). A proportionality is indicated by dotted lines.

4.2.2. Fluence and wavelength dependence

As already obvious from Fig. 4.4, the laser fluence $\langle F \rangle$ absorbed by the O/C/Ru(001) surface has a strong influence on the resulting desorption yield. Therefore, the fluence dependence was investigated systematically for two different wavelengths of the fs-laser pulses. The results obtained for irradiating a O/C/Ru(001) surface with $\theta_C = 0.04$ ML with absorbed fluences ranging from 100 to 200 J/m^2 are shown in Fig. 4.5. A non-linear increase of the desorption yield Y with increasing absorbed laser fluence $\langle F \rangle$ is observed. The yield-weighted fluence $\langle F \rangle$ is calibrated self-consistently via this measurement as explained in the beginning of Section 2.5. The fluence dependencies for both wavelengths are well reproduced by a power law given via

$$Y \propto \langle F \rangle^n \quad \text{with } n = \begin{cases} 3.9 \pm 0.4 & \text{for } 400\,\text{nm} \\ 4.3 \pm 0.2 & \text{for } 800\,\text{nm} \end{cases} . \tag{4.2}$$

Excitation with 400 nm light leads to higher reaction yields Y than excitation with 800 nm light does for the same absorbed fluence. This effect is also included in the decay curves depicted in Fig. 4.6. There, the associative CO desorption yield from a O/C/Ru(001) surface with an initial carbon coverage θ_C=0.04 ML as a function of applied laser shots is shown. Data sets for several absorbed fluences $\langle F \rangle$ for each of the two applied wavelengths are presented in Fig. 4.6(a) and (b) for 400 and 800 nm light, respectively. For both wavelengths, it can be seen that higher laser fluences result in a faster decay of the desorption yield, which means that the surface is depleted with less laser pulses resulting in a higher first shot yield. This means that the faster decay for excitation with 400 nm than 800 nm light at comparable fluences as shown in Fig. 4.6 also indicates the enhanced desorption yield obvious in Fig. 4.5. Before discussing possible origins of this effect, a more quantitative analysis in terms of the determination of the reaction cross sections for the associative desorption will be performed.

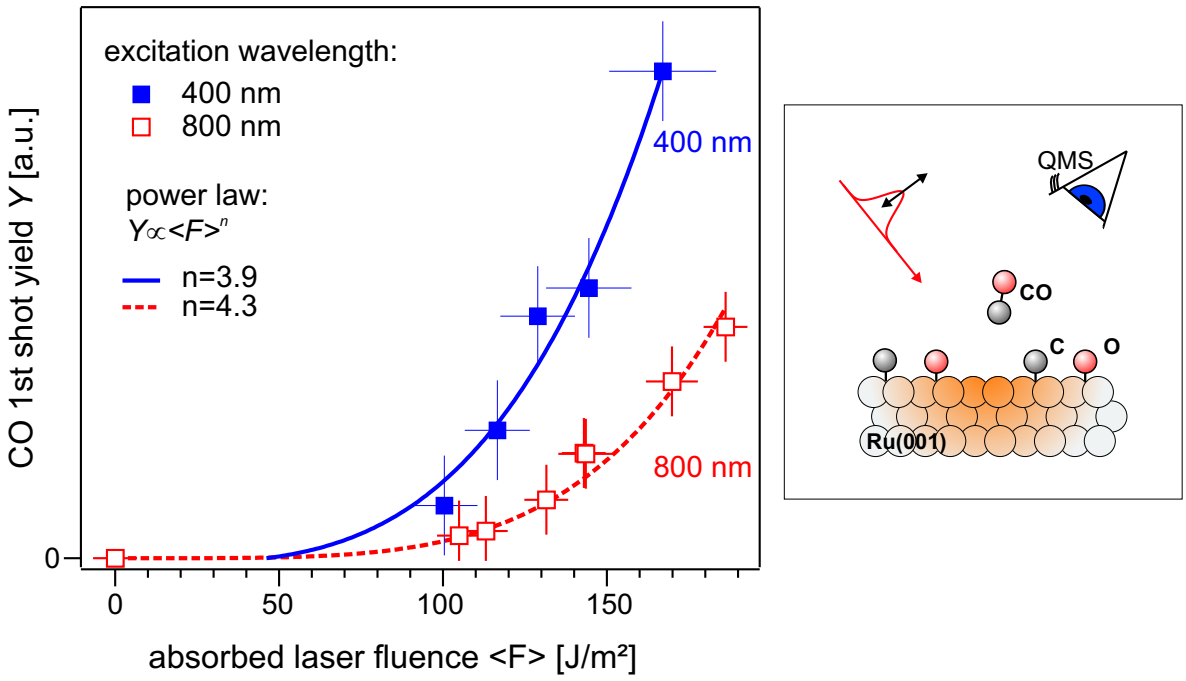

Figure 4.5.: Fluence dependence of the CO reaction yield Y obtained from a O/C/Ru(001) surface with carbon pre-coverage of θ_C=0.04 ML. Y was measured as a function of absorbed fluence $\langle F \rangle$ for two different excitation wavelengths of 400 and 800 nm. The lines represent fits by a power law: $Y \propto \langle F \rangle^n$.

Cross section of the fs-laser induced associative CO desorption

The efficiency of the recombination process can be quantified in terms of the reaction cross section. Therefore, one analyzes the decay of the reaction yield Y as a function of the number i of laser pulses irradiated onto the surface [Kao93a, Fun00]. If it is assumed that the photodesorbed CO signal Y_i due to the i-th laser pulse is proportional to the change of coverage $\Delta\theta_i$, and this change is proportional to the coverage θ_i, one then has

$$Y_i \propto \Delta\theta_i = \theta_i \, f(F_i), \tag{4.3}$$

where $f(F_i)$ is a general functional dependence of the desorption yield on fluence. Equation (4.3) represents a first order process, whereas $\Delta\theta_i \propto \theta_i^2$ is suited to describe second order processes. For the case of a *linear* fluence dependence, $f(F_i)$ is simply given by σF_i, where σ is the reaction cross section. Summation in Eq. (4.3) then yields

$$\theta_i^{\mathrm{lin}} = \theta_0 \, \mathrm{e}^{-\sigma F_i} \quad \text{with } F_i = \sum_{j=0}^{i} F_j, \tag{4.4}$$

where θ_0 is the initial coverage and F_j the fluence of the j-th laser pulse. In case of a *non-linear* dependence of the yield on fluence, $f(F_i) = \beta F_i^n$, θ_i can again be obtained by integrating Eq. (4.3),

$$\theta_i^{\mathrm{nl}} = \theta_0 \, \mathrm{e}^{-\beta F_i^{\mathrm{eff}}} \quad \text{with } F_i^{\mathrm{eff}} = \sum_{j=0}^{i} F_j^n, \tag{4.5}$$

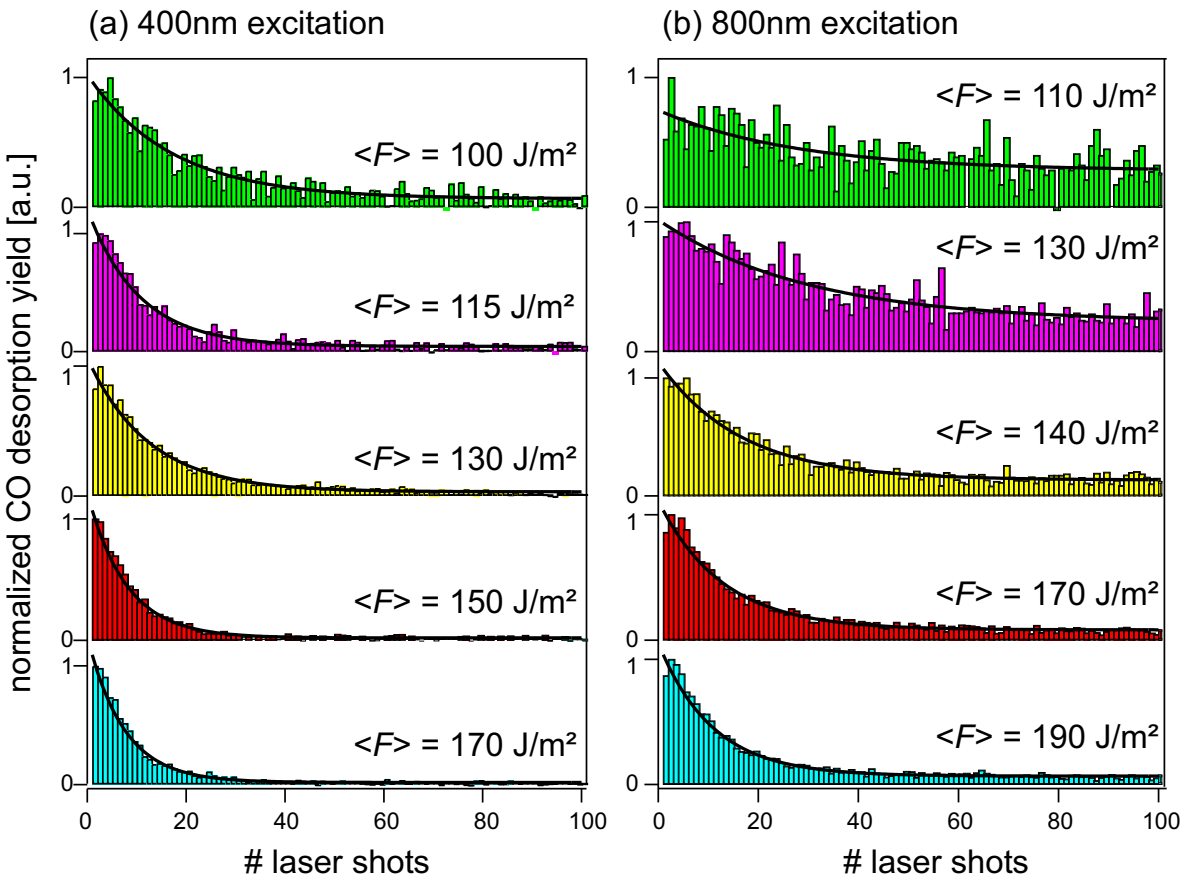

Figure 4.6.: Decay of the associative CO desorption yield from a O/C/Ru(001) surface with an initial carbon coverage θ_C=0.04 ML as a function of the laser shot number within a series of 100 pulses. Data sets for excitation with (a) 400 and (b) 800 nm laser light are shown. The solid lines represent fits of Eq. (4.5) to the experimental data. Note the faster decay for excitation with 400 nm than 800 nm light at comparable absorbed fluences $\langle F \rangle$.

where n is the exponent of the power law and β is a scaling constant. The effective cross section is then defined as

$$\sigma_{\text{eff}} = \beta \frac{\sum_i F_i^n}{\sum_i F_i}, \tag{4.6}$$

which simplifies for pulses of identical fluence (F_i=F=const.) to

$$\sigma_{\text{eff}} = \beta F^{n-1}. \tag{4.7}$$

For the associative CO desorption, this effective cross section σ_{eff} is determined by fits of Eq. (4.5) to the experimental data depicted in Fig. 4.6. Since the decay curves are induced by laser pulses of the same fluence, a linear dependence exists between the number of laser pulses i and the accumulated effective fluence F_i^{eff}, which allows to plot the decay curve with i as abscissa for a more clear illustration. As can be seen from Fig. 4.6, the experimental data are well reproduced by a single exponential decay indicating that the desorption can be accurately described by a single cross section. This justifies the use of Eq. (4.3) for the presented analysis, which represents a first-order desorption behavior. A second order process would however change Eq. (4.5) to an inverse power law [Den04], which does not reproduce

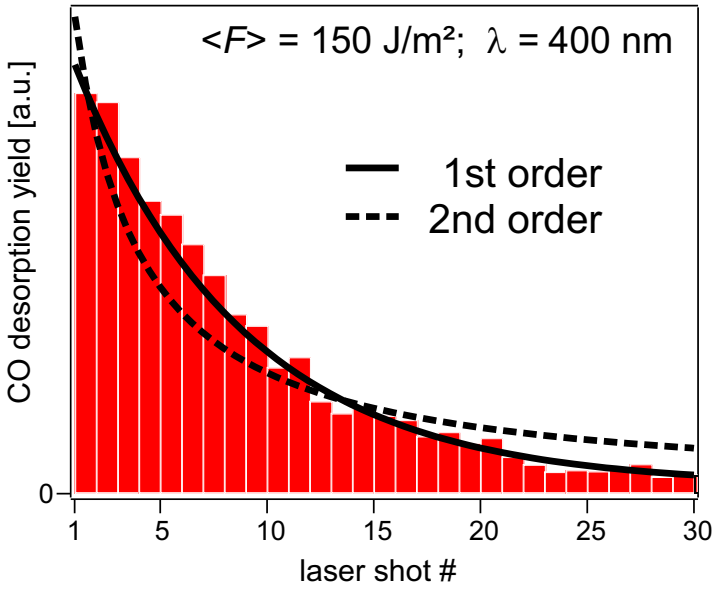

Figure 4.7.: Decay curve of fs-laser induced CO desorption yield. The experimental parameters are $\langle F \rangle = 150\,\mathrm{J/m^2}$, excitation wavelength $\lambda = 400\,\mathrm{nm}$ and $\theta_C = 0.04\,\mathrm{ML}$. Fits for an assumed first and second order process are depicted by a solid and a dashed line, respectively.

the experimental data as can be seen from Fig. 4.7. Thus, it is evidenced that the associative CO recombination under the present conditions can be described as a first order process.

For an absorbed laser fluence of $\langle F \rangle$=170 J/m^2, an effective cross section for the fs-laser induced associative CO desorption of

$$\sigma_{\mathrm{eff}} = \begin{cases} 4.9(3) \cdot 10^{-18}\ \mathrm{cm}^2 & \text{for } 400\,\mathrm{nm} \\ 1.1(2) \cdot 10^{-18}\ \mathrm{cm}^2 & \text{for } 800\,\mathrm{nm} \end{cases} \tag{4.8}$$

is determined.

Typical cross sections for photon induced desorption of neutrals from surfaces lie in the range from 10^{-18} to $10^{-20}\,\mathrm{cm}^2$ [Mad86]. For the desorption of molecular CO from Ru(001), a σ_{eff} of $5.3 \cdot 10^{-18}\,\mathrm{cm}^2$ was determined for the excitation with 800 nm fs-laser pulses and an absorbed flunce $\langle F \rangle = 190\,\mathrm{J/m^2}$ [Fun00][4]. The approximately same absorbed fluences allow to compare the cross sections directly. This means that the fs-laser induced desorption of molecularly bound CO is ≈ 5 times more efficient than desorption of its atomically bound counterpart.

With the effective cross sections, the CO desorption probability per pulse can be determined via $P_{\mathrm{des}} = \sigma_{\mathrm{eff}}\ \langle F \rangle$. For an absorbed fluences $\langle F \rangle$ of $170\,\mathrm{J/m^2}$ desorption probabilities of 0.17 and 0.07 are obtained for excitation with 400 and 800 nm laser wavelength, respectively. For an initial coverage of $\theta_C \approx 0.04\,\mathrm{ML}$, approximately 7‰ and 3‰ of a ML CO are thus formed due to the irradiation of a single laser pulse. Possible origins for the factor of ≈ 2 between σ_{eff} for 400 and 800 nm light will be discussed in the following.

[4]It has to be noted that in [Fun00] an effective cross section of $\sigma_{\mathrm{eff}} = 1.7 \cdot 10^{-18}\,\mathrm{cm}^2$ for an absorbed fluence of $\langle F \rangle = 305\,\mathrm{J/m^2}$ is given. However, the absorbed fluences given in this reference are inconsistent with the given incident fluences and the reflectivity of Ru(001). Most probably, the absorbed and reflected fluences are interchanged. This seems pretty likely, since absorbed fluences $\geqq 300\,\mathrm{J/m^2}$ are far above the damage threshold of Ru. Hence, the experimental data is re-analyzed, wherefrom the higher cross section for a lower absorbed fluence results.

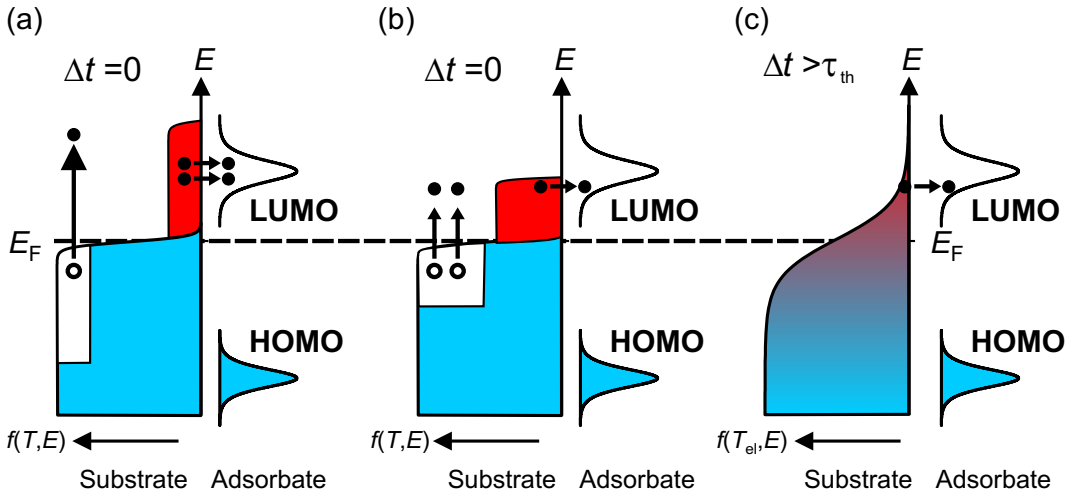

Figure 4.8.: Illustration of the wavelength-dependent non-equilibrium distribution directly after optical excitation of a metal with an ultrashort laser pulse (Δt=0). The same amount of absorbed energy leads to (a) less but more strongly excited electrons for higher photon energies than it does for (b) lower photon energies. The higher density of high-energetic electrons after excitation with the shorter wavelength may couple more efficiently to unoccupied adsorbate resonances (LUMO), which may strongly influence the efficiency of the investigated surface reaction. (c) Due to thermalization of the electron distribution ($\Delta t > \tau_{\mathrm{th}}$), the wavelength dependent peculiarities vanish.

Possible origins of the wavelength dependence

The pronounced enhancement of the associative CO desorption yield after fs-laser excitation with 400 nm laser pulses compared to excitation with 800 nm light, can have several origins.

As illustrated in Fig. 4.8(a) and (b), an ultrashort laser pulse creates a highly non-thermal, nascent carrier distribution, which before thermalization depends strongly on the photon energy of the applied light pulse. Assuming laser pulses of same overall energy but different photon energies, a distribution of less but more energetic non-thermal electrons is obtained from excitation with the shorter wavelength[5]. The higher density of more-energetic electrons may couple more efficiently to unoccupied adsorbate resonances (LUMO), which may strongly influence the efficiency of the investigated surface reaction. Due to thermalization of the electron distribution, the wavelength dependent difference vanishes for times larger than the thermalization time τ_{ph} (Fig. 4.8c). Concerning the present experiment, a photon energy of 3.1 eV for 400 nm light is twice as high as the 1.55 eV for a 800 nm photon. This means, if an unoccupied adsorbate resonance responsible for the associative CO desorption lies between 1.55 and 3.1 eV above the Fermi level, the reaction yield is greatly enhanced for excitation with 400 nm light. This enhancement will result in less excitation steps required for the transfer of sufficient energy into the responsible reaction coordinate. Thus, a smaller exponent n for the power law describing the fluence dependence should be observed for excitation with more energetic photons. Such a behavior was found for the O_2 desorption and CO_2 formation after fs-laser irradiation of a O_2/CO/Pt(11) surface [Kao93a, Del95]. The exponents of the power law describing the observed fluence dependencies differed by a factor of two with the lower value representing excitation with twice the photon energy. These findings are in contrast

[5]Note that multi-photon excitation is neglected in this illustrative description, since it is not required for a qualitative understanding of this aspect of wavelength dependency.

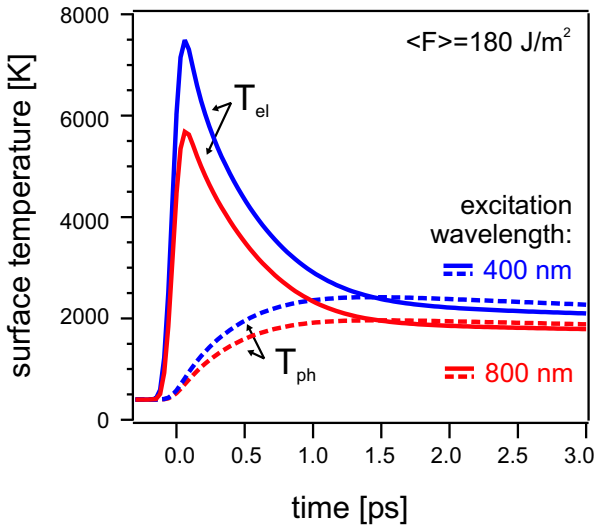

Figure 4.9.: Calculated surface temperatures obtained from the two-temperature model as a function of time after fs-laser excitation. An absorbed fluence of 180 J/m^2 for the two applied wavelengths of 400 and 800 nm light leads to significantly higher electron and phonon temperatures T_{el} and T_{ph} for the shorter wavelength.

to the marginally lowered exponent determined for the fs-laser induced CO recombination presented here.

Another origin for the observed effect might be the different optical properties of the Ru(001) substrate with respect to the two applied wavelengths. As shown in Table 1.1, the penetration depth for 800 nm light is more than twice as large as for 400 nm light meaning that the energy of the 400 pulses is absorbed closer to the surface. Figure 4.9 depicts the electron and phonon surface temperatures T_{el} and T_{ph} after fs-laser excitation of the Ru(001) substrate with laser pulses of different wavelength but same absorbed fluence. The calculations are performed within the framework of the two-temperature model (Section 1.2) and the only difference, which is taken into account, is the different penetration depth δ for the two wavelengths, which is 6.9 and 16.2 nm for 400 and 800 nm, respectively. Significantly higher surface temperatures for both the electron and the phonon heat bath are obtained after excitation with the shorter wavelength. The resulting higher adsorbate temperatures T_{ads} lead to an enhancement of the reaction yield due to its Arrhenius-like nature. Thus, an enhanced reaction yield resulting from an excitation with 400 instead of 800 nm laser pulses is expected.

Summarizing one has to state that the enhancement of the associative CO desorption yield observed after excitation of the O/C/Ru(001) surface with 400 nm fs-laser pulses compared to excitation with 800 nm pulses can have several reasons. The enhancement can either results from the different optical penetration depths δ leading to higher electron and phonon surface temperatures or from the different non-thermal electron distributions directly after optical excitation. The latter seems to be unlikely, since no distinct difference in the exponent of the power law describing the fluence dependence is found. In addition, the very rapid thermalization of the non-thermal electron distributions reduces the available interaction time to ≈ 100 fs (see Section 1.2.1), which makes the process also rather implausible.

4.2.3. Two pulse correlation

A determination of the reaction mechanism being responsible for the fs-laser induced associative desorption of CO from O/C/Ru(001) is not possible with the results presented in the preceding sections, whereas the measurement of a two-pulse correlation (2PC) can reveal this information. Due to the non-linearity of the desorption yield on the absorbed laser fluence, a split into two laser pulses with a certain time delay Δt allows to probe how long the second laser pulse benefits from irradiating the system with the first pulse. Results for a carbon coverage of $\theta_C = 0.04\,\mathrm{ML}$ are shown in Fig. 4.10. The total absorbed fluence of $\langle F \rangle = 170\,\mathrm{J/m^2}$ at a wavelength of 800 nm is the sum of both pulses, which have a fluence ratio of 55/45. Negative delays indicate that the stronger pulse precedes. A full width at half maximum of

$$\mathrm{FWHM_{2PC}} \approx 20\,\mathrm{ps} \tag{4.9}$$

for the correlation measurement is found. This finding clearly rules out any exclusive ultrafast electron mediated reaction mechanism with coupling times shorter than the electron-phonon coupling of the Ru(001) substrate. This implies that the observed wavelength dependence can not originate from a mechanism based on non-thermalized electrons, since the thermalization time is in the order of the laser-pulse duration, i.e. ∼100 fs (see Section 1.2.1). "Slow" electron mediated reaction mechanisms with coupling times larger than the electron-phonon equilibration time can not be resolved within a 2PC scheme, since the thermal non-equilibrium of the two heat baths can no longer be experienced by the adsorbate. Therefore, the experimental outcome of the 2PC measurement has to be discussed carefully as will be done in Section 4.4.

In addition to the FWHM, the 2PC also reveals the exponent of the fluence dependence, since at large pulse-pulse delays Δt the two pulses do not benefit from each other anymore and

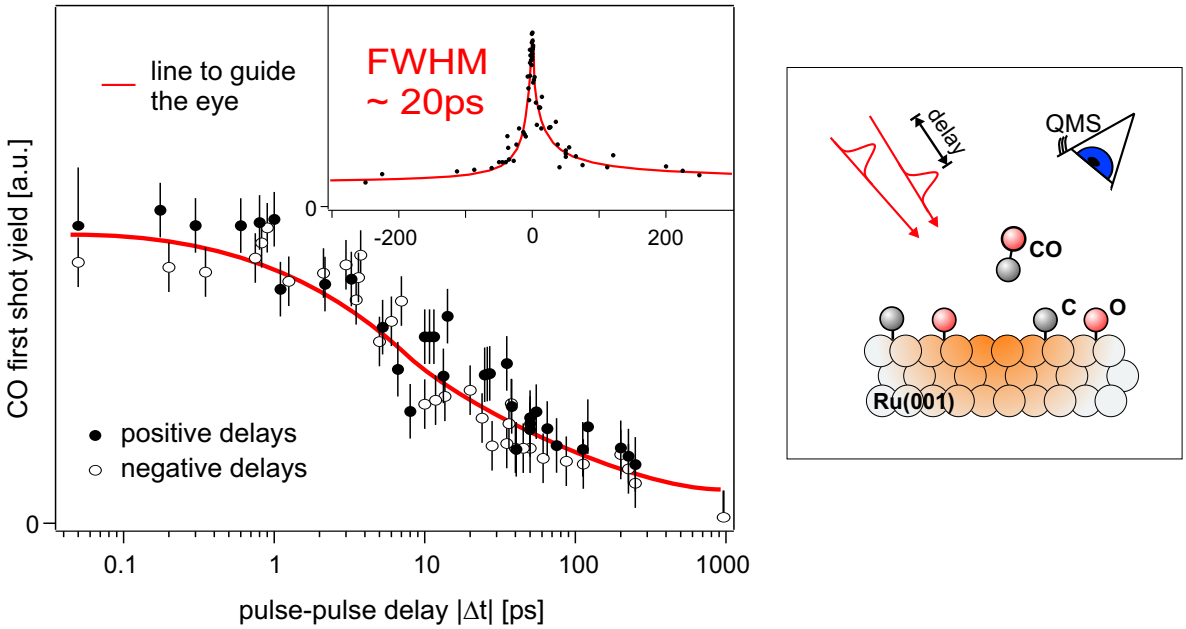

Figure 4.10.: Two-pulse correlation measurement of CO desorbing associatively from Ru(001). The reaction yield is measured as a function of the pulse-pulse delay Δt between two 800 nm fs-laser pulses, whose fluences of ratio 55/45 add up to a total absorbed fluence of $\langle F \rangle = 170\,\mathrm{J/m^2}$. Negative delays indicate that the stronger precedes. The line is a guide to the eye. (Note the logarithmic scale of the time-axis in the main graph.)

the measured yield is $Y \propto 2 \cdot \langle F \rangle^n$. At $\Delta t = 0$ a yield corresponding to an excitation with a single pulse of twice the fluence results. Thus, the ratio between the yield of the peak and the wings determines the exponent of the fluence dependence via

$$\frac{Y(2\langle F \rangle)}{2Y(\langle F \rangle)} = \frac{(2\langle F \rangle)^n}{2(\langle F \rangle)^n} = \frac{1}{2} \cdot 2^n. \tag{4.10}$$

An exponent of $n = 3.6$ is obtained, which is slightly lower than the $n = 4.3$ given in Section 4.2.2 for excitation with 800 nm pulses. This deviation can be rationalized, if one considers that according to the 2TM it takes ≈ 500 ps until the surface temperature has fully cooled down to its initial value. Thus, only for $|\Delta t| > 500$ ps the succeeding pulse does not benefits from its preceding cousin. This means that the denominator of Eq. (4.10) might be slightly too large, which results in a too small exponent n.

Taking into account the power law describing the fluence dependence, one can calculate the desorption yield for an infinite delay between the two laser pulses. The outcome of this calculation is depicted as the data point at $\Delta t = 1000$ ps in Fig. 4.10. It is slightly lower than the experimentally determined wings, but still overlapping within the error bars.

4.2.4. Isotope effect

As explained in Section 1.3.3 and Section 3.3, an isotope effect concerning the fs-laser induced desorption yield would be an indication for an electron mediated reaction mechanism and represents therefore another possibility to distinguish between a "slow" electron mediated and a phonon mediated reaction mechanism.

Therefore, the surface was prepared as described in Section 2.5.2 with mixtures of isotopically marked oxygen and carbon, respectively. Decay curves of the CO desorption yield after excitation with fs-laser pulses of 800 nm wavelength and an absorbed fluence of $\langle F \rangle = 180\,\mathrm{J/m^2}$

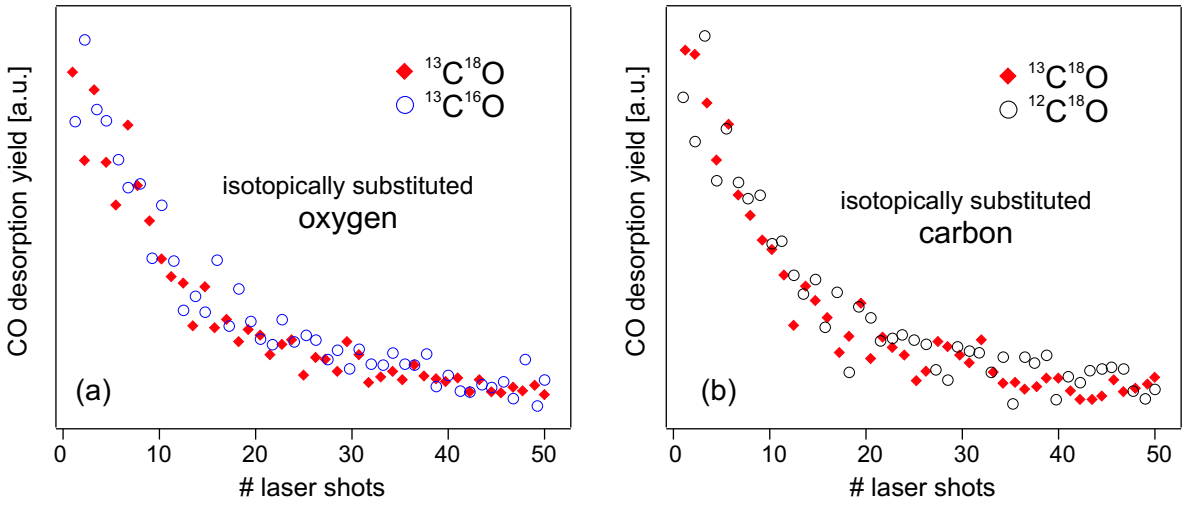

Figure 4.11.: Decay curves of the CO yield as a function of laser shot number for laser pulses of 800 nm wavelength and an absorbed fluence of $\langle F \rangle = 180\,\mathrm{J/m^2}$. The CO yield is measured for isotopically substituted reactants, (a) ^{16}O and ^{18}O and (b) ^{12}C and ^{13}C.

are depicted in Fig. 4.11. The reaction yield is determined for isotopically substituted reactants. Fig. 4.11(a) shows the decay curve of $^{13}C^{16}O$ and $^{13}C^{18}O$, whereas Fig. 4.11(b) shows the decay curve of $^{12}C^{18}O$ and $^{13}C^{18}O$. As already obvious from the figure, no pronounced isotope effect is found and a quantitative analysis results in ratios for the desorption yield Y of

$$\frac{Y(^{13}C^{16}O)}{Y(^{13}C^{18}O)} = 1.05(6) \quad \text{and} \quad \frac{Y(^{12}C^{18}O)}{Y(^{13}C^{18}O)} = 0.97(6). \tag{4.11}$$

In the fs-laser induced oxidation experiments of CO+O on Ru(001) by Bonn et al. [Bon99], a pronounced isotope effect from a $^{16}O/^{18}O$/CO coadsorbate system was found resulting in a oxidation yield ratio of $Y(^{16}OCO)/Y(^{18}OCO) \approx 2.4$, whereas the isotopical substitution of the CO reactant did not show an isotope effect. Thus, the activation of the oxygen atom could be determined as the rate limiting step of an electron mediated surface reaction.

On the other hand, a non-observable isotope effect does not necessarily mean that the fs-laser induced CO recombination is not electron mediated. If one reconsiders that the PES governing the CO recombination on Ru(001) exhibits the barrier mainly along the intramolecular coordinate d [Mav98], it is clear that the reduced mass μ of the molecule has to be taken into account regarding a possible isotope effect. The change in μ due to isotopical substitution is only 5%. A therefrom resulting isotope effect could be hidden within the error bars of our experimental findings and will hence be discussed carefully further below.

4.2.5. Time-of-flight measurements

To characterize the energy release into the reaction products, the translational energy of the desorbing CO molecules along the surface normal is measured. The recorded spectra for various absorbed laser fluences $\langle F \rangle$ of laser pulses with 400 and 800 nm wavelength are depicted in Fig. 4.12. The initial surface temperature T_S of the Ru crystal is 400 K and $\theta_C = 0.04$ ML. The experimental data is well reproduced by single modified Maxwell-Boltzmann distributions. The descriptiveness of the data sets with single distributions suggests that the desorption process occurs via a single reaction channel and allows to reproduce the experimental data with a single temperature $T_{trans} = \langle E \rangle / 2k_B$. The flight times for the CO molecules desorbing after excitation with 400 (Fig. 4.12a) and 800 nm (Fig. 4.12b) fs-laser pulses decrease only moderate with increasing laser fluence. The measured T_{trans} range from 600 to 860 K. Slightly higher translational temperatures T_{trans} are obtained after excitation with 400 instead of 800 nm light. This difference will be discussed in Section 4.4.

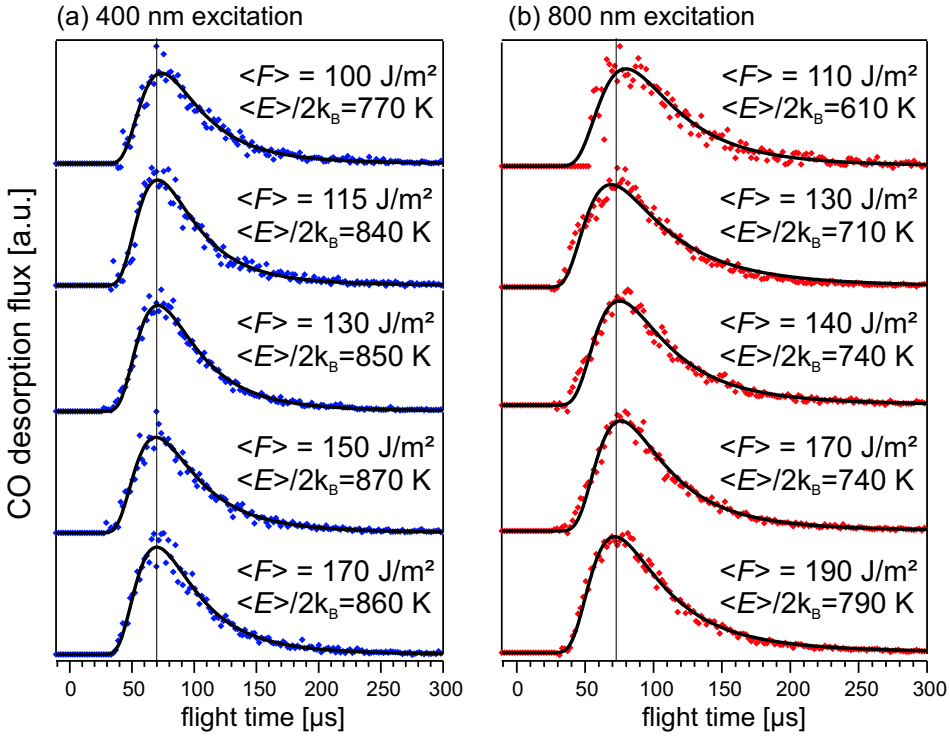

Figure 4.12.: Time-of-flight distributions of CO desorbing associatively from Ru(001) (T_S = 400 K) after irradiation with (a) 400 nm and (b) 800 nm fs-laser pulses of various absorbed fluences $\langle F \rangle$. Solid lines are modified Maxwell-Boltzmann distributions for the given temperatures $\langle E \rangle / 2k_B$. The dashed lines are guide to the eye to clarify the very moderate decrease in flight time with increasing fluence.

4.3. Modeling the associative CO desorption

Since no unambiguous direct experimental indication for either an electron or a phonon mediated CO recombination reaction is found as shown in the previous sections, the data are analyzed in the framework of the frictional approach explained in detail in Section 1.3.

The fluence dependencies for the two applied wavelengths and the two-pulse correlation are simultaneously modeled with parameter sets consisting of the coupling coefficients to the electron and phonon heat bath η_{el} and η_{ph}, respectively, and an activation energy E_{a}. The coupling strengths are treated as *fit parameters*, whereas a *fixed* activation energy E_{a} obtained from the TDS measurements presented in Section 4.1.3 is used. The experimental data are expressed in coverage-independent terms of desorption probabilities P_{des} obtained from the cross sections determined in Section 4.2.2. Thus, the measured and modeled *absolute* yields can be directly compared.

Before discussing the details of different parameter sets applied to model the data, one fact similar in all modeled scenarios has to be mentioned: the wavelength dependence of the reaction yield concerning excitation with 400 and 800 nm fs-laser pulses is well reproduced by the applied friction model, taking solely into account the different penetration depths in the used two-temperature model. This means that the energy absorption closer to the Ru(001) surface for the shorter wavelength accounts for the observed enhanced reaction yield. An explanation taking into account the initially higher energetic electrons has not to be considered. The latter can be excluded from the observed 2PC width of ≈ 20 ps as discussed in Section 4.2.3.

Furthermore, a purely electron mediated reaction with coupling times shorter than the electron-phonon equilibration time of $\tau_{\mathrm{el-ph}} = 1.6$ ps for Ru(001) [Fun00] can also be excluded, since this typically leads to 2PC widths narrower than 5 ps [Bon00a, Den03b]. The outcome of purely electronic scenarios with $\eta_{\mathrm{el}}^{-1} = \tau_{\mathrm{el}} > \tau_{\mathrm{el-ph}}$ is almost identical to a pure phonon scenario. This ambiguity lies inherently in the model, since the thermal non-equilibrium between the electron and the phonon heat baths can no longer be experienced by the adsorbate. Thus, solely the outcome of a purely phonon mediated scenario ($\eta_{\mathrm{el}} = 0$, i.e. $\tau_{\mathrm{el}} = \infty$) and a scenario considering both, electron and phonon coupling, will be discussed in the following.

Since the activation energy E_{a} is not unambiguously determinable from the TDS data as long as the pre-exponential factor ν is unknown (see Section 4.1.3), barrier heights of $E_{\mathrm{a}} = 1.5$ eV obtained for a "normal" pre-exponential $\nu \sim 10^{13}\,\mathrm{s}^{-1}$ from Eq. (4.1) and a significantly lower $E_{\mathrm{a}} = 1.0$ eV corresponding to $\nu \sim 10^{9}\,\mathrm{s}^{-1}$ are considered to investigate the influence of the barrier height onto the predictions of the model.

Three different scenarios will be discussed. The best fit values for η_{el}^{-1} and η_{ph}^{-1} obtained for modeling the three scenarios are given in Table 4.1. The outcome of the modeling is depicted in Fig. 4.13 together with the experimental data and the peculiarities of the different scenarios will be discussed in the following regarding qualitative and quantitative agreement.

Qualitative agreement

Scenario A describes an electron and phonon mediated reaction mechanism with an activation energy $E_{\mathrm{a,TDS}} = 1.5$ eV. Best fits are obtained with $\eta_{\mathrm{el}}^{-1} = 0.5$ ps and $\eta_{\mathrm{ph}}^{-1} = 1.2$ ps. As can

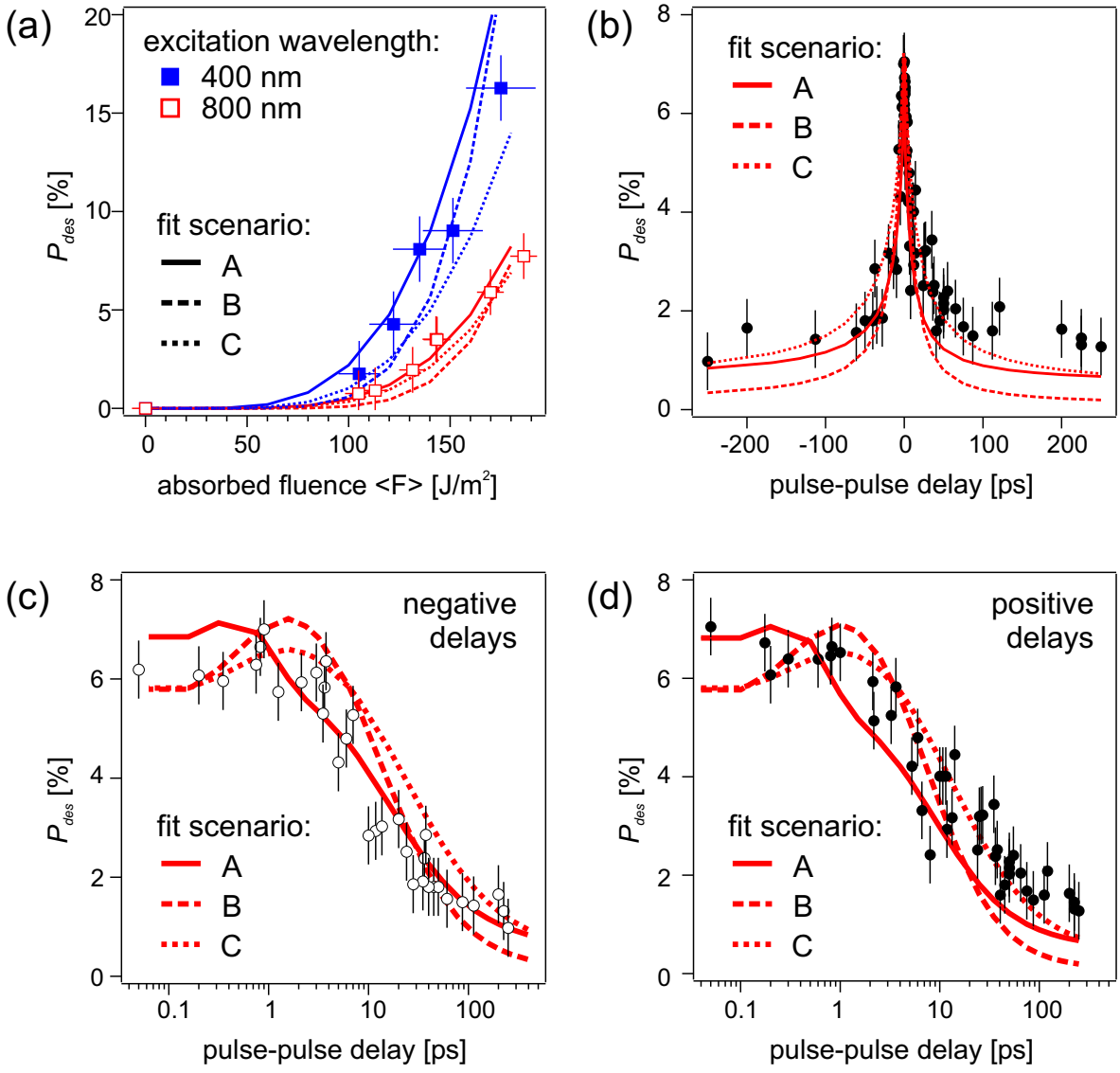

Figure 4.13.: Modeling of the associative CO desorption in the framework of a frictional approach. Experimental and modeled data is shown for (a) the fluence dependence for the two applied fs-laser wavelengths of 400 and 800 nm and (b) the two-pulse correlation measurement. Panels (c) and (d) depict the 2PC on a logarithmic timescale for clarity. Modeled data for three types of parameter sets denoted A, B and C are depicted by dotted, dashed and solid lines, respectively. The fit parameters are as follows:
scenario A - electron and phonon mediated: $\eta_{\mathrm{el}}^{-1} = 0.5\,\mathrm{ps}$, $\eta_{\mathrm{ph}}^{-1} = 1.2$ ps and $E_{\mathrm{a}} = 1.5\,\mathrm{eV}$
scenario B - purely phonon mediated: $\eta_{\mathrm{el}} = 0$, $\eta_{\mathrm{ph}}^{-1} = 1.2$ ps and $E_{\mathrm{a}} = 1.5\,\mathrm{eV}$
scenario C - purely phonon mediated: $\eta_{\mathrm{el}} = 0$, $\eta_{\mathrm{ph}}^{-1} = 1.2$ ps and $E_{\mathrm{a}} = 1.0\,\mathrm{eV}$

be seen from Fig. 4.13(a), the fluence dependencies are well described with values slightly too high for the 400 nm wavelength data. The modeling of the 2PC data depicted in Fig. 4.13(b) results in a FWHM of ≈ 17 ps. The wings at delays $|\Delta t| > 100$ ps are in reasonable agreement with the experimental data. The logarithmic scales of Fig. 4.13(c+d), reveal that the shape of the 2PC is well reproduced at negative delays, whereas at positive delays values slightly too low are obtained causing a smaller peak width than observed in the experiment. In summary, the outcome of the friction model considering non-adiabatic coupling reproduces the experimental data to a reasonable degree.

This changes completely, if one tries to model the data taking into account only adiabatic coupling and a barrier height of 1.5 eV. This is done with **scenario B**. Best fits are obtained for $\eta_{\mathrm{ph}}^{-1} = 1.2$ ps. Although the fluence dependencies are well described, it is not possible to reproduce the 2PC data. A FWHM of ≈ 20 ps can still be modeled, whereas the desorption probability for pulse-pulse delays larger than ± 50 ps is way too low as can be seen in Fig. 4.13(b).

Scenario C describes also purely adiabatic coupling to the phonons, but takes into account an activation energy of 1.0 eV which is significantly lower than the one used in scenarios A and B. Figure 4.13(a) shows that the fluence dependencies are well described, with values slightly too low for the 400 nm data. The baseline of the 2PC is reproduced in agreement with the experimental data and the shape of the 2PC is also described reasonable well with slightly too high values for negative delays leading to an increased FWHM of ≈ 28 ps.

This means that the experimental data is *qualitatively* well reproduced considering either non-adiabatic coupling and an activation energy of 1.5 eV or taking into account a lower barrier height of 1.0 eV and exclusive adiabatic adsorbate-substrate coupling. A purely phonon mediated reaction mechanism with an activation energy of 1.5 eV can be excluded, since it does not reproduce the experimental data.

Quantitative agreement

As explained in detail in Section 1.3.2, the applied friction approach is capable of modeling *absolute* reaction rates via Eq. (1.42) and Eq. (1.44). The ratios of the experimentally determined reaction yields Y_{exp} and the modeled Y_{mod} are denoted for each model scenario in Table 4.1. Excellent agreement is found for scenarios A and C, whereas the modeled yield of scenario B is one order of magnitude too low.

modeled reaction scenario	E_{a}	η_{el}^{-1}	η_{ph}^{-1}	$Y_{\mathrm{exp}}/Y_{\mathrm{mod}}$	$\nu_{\mathrm{mod}}^{\mathrm{RW}}$
A: electron and phonon mediated	1.5 eV	0.5 ps	1.2 ps	2	$2.2{\cdot}10^{13}\,\mathrm{s}^{-1}$
B: purely phonon mediated	1.5 eV	∞	1.2 ps	17	$0.9{\cdot}10^{13}\,\mathrm{s}^{-1}$
C: purely phonon mediated	1.0 eV	∞	1.2 ps	1	$0.6{\cdot}10^{13}\,\mathrm{s}^{-1}$

Table 4.1.: Overview of the different reaction scenarios modeled within the framework of a frictional approach to reproduce the experimental data of the fs-laser induced CO recombination. The activation energy E_{a} is kept fixed, whereas the coupling times η_{el}^{-1} and η_{ph}^{-1} are used as *fit parameters*. Best fit values for each data set are given. $Y_{\mathrm{exp}}/Y_{\mathrm{mod}}$ denotes the ratio between experimentally determined and modeled reaction yields. $\nu_{\mathrm{mod}}^{\mathrm{RW}}$ gives rate-weighted mean pre-exponentials obtained for Kramer's low friction limit.

As long as Kramers' low friction limit applies, the pre-exponential of the Arrhenius-like expression can be obtained via

$$\nu = (\eta_{\mathrm{el}} + \eta_{\mathrm{ph}}) \cdot E_{\mathrm{a}}/k_{\mathrm{B}}T_{\mathrm{ads}}. \tag{4.12}$$

Since the adsorbate temperature T_{ads} is transient during the reaction a mean temperature representing the adsorbate heat bath, namely the rate-weighted adsorbate temperature $T_{\mathrm{ads}}^{\mathrm{RW}}$ is introduced as

$$T_{\mathrm{ads}}^{\mathrm{RW}} = \frac{\int R(t) \cdot T_{\mathrm{ads}}(t)\,\mathrm{d}t}{\int T_{\mathrm{ads}}(t)\,\mathrm{d}t}. \tag{4.13}$$

This means that $T_{\mathrm{ads}}(t)$ contributes to $T_{\mathrm{ads}}^{\mathrm{RW}}$ according to its respective reaction rate $R(t)$. A rate-weighted adsorbate temperatures of 2250 K is obtained for scenario A and $T_{\mathrm{ads}}^{\mathrm{RW}} = 1550\,\mathrm{K}$ is obtained for scenario B and C. The higher $T_{\mathrm{ads}}^{\mathrm{RW}}$ for scenario A results from the high temperatures of the electron heat bath directly after fs-laser excitation which couples non-adiabatically to the adsorbate, whereas in scenario B and C only adiabatic coupling to the colder phonon heat bath is considered. With $T_{\mathrm{ads}}^{\mathrm{RW}}$, η_{el}, η_{ph} and E_{a}, a rate-weighted pre-exponential $\nu_{\mathrm{mod}}^{\mathrm{RW}}$ can now be calculated via Eq. (4.13). Values of $\nu_{\mathrm{mod}}^{\mathrm{RW}} \sim 10^{13}\,\mathrm{s}^{-1}$ are obtained for all three modeled scenarios and the explicit values are given in Table 4.1. The similarity of $\nu_{\mathrm{mod}}^{\mathrm{RW}}$ for all three scenarios is due to similar frictional coupling strengths dominating the order of magnitude for ν, which are predetermined by the width of the measured 2PC.

As discussed before, the activation energy E_{a} is obtained from TDS data as a function of the pre-exponential, which will in the following be denoted ν_{TDS}. For $E_{\mathrm{a}} = 1.5\,\mathrm{eV}$, ν_{TDS} and $\nu_{\mathrm{mod}}^{\mathrm{RW}}$ exhibit the same order of magnitude of $\sim 10^{13}\,\mathrm{s}^{-1}$. This means that for $E_{\mathrm{a}} = 1.5\,\mathrm{eV}$, the thermal and the fs-laser induced CO recombination can be consistently described within the applied low friction limit.

In contrast, an activation energy of $E_{\mathrm{a}} = 1.0\,\mathrm{eV}$ corresponds to $\nu_{\mathrm{TDS}} \sim 10^{9}\,\mathrm{s}^{-1}$, which is four orders of magnitude smaller than $\nu_{\mathrm{mod}}^{\mathrm{RW}}$. This means that for $E_{\mathrm{a}} = 1.0\,\mathrm{eV}$ the pre-exponential can not be expressed via Eq. (4.12) in the low friction limit. The underlying idea of the low friction limit is that the reaction rate-limiting step is the energy transfer to the adsorbate and not the pre-exponential ν_0 obtained from TST. In the applied 1D model, the energy is automatically coupled into the coordinate relevant for reaction, whereas in multi-dimensional dynamics the energy is not exclusively transferred into the reaction coordinate but also into dimensions not responsible for the reaction. Thus, a lower multidimensional pre-exponential results. The experimentally determined ν_{TDS} includes the multi-dimensionality of the desorption process and can thus be applied for modeling absolute reaction rates under the assumption that the fs-laser induced desorption is in thermal equilibrium to the same extent as the thermal desorption. This can be considered as an upper limit for the reaction rate, since processes far off from equilibrium conditions (e.g. fs-laser induced desorption) can lead to a significant decrease of ν [Gri81a, Tul81]. Since ν_{TDS} is four orders of magnitude smaller than $\nu_{\mathrm{mod}}^{\mathrm{RW}}$ for $E_{\mathrm{a}} = 1.0$, the modeled reaction rate considering the multi-dimensional ν_{TDS} is also four orders of magnitude smaller and $Y_{\mathrm{exp}}/Y_{\mathrm{mod}} \sim 10^4$. In contrast, considering a barrier height of $E_{\mathrm{a}} = 1.5\,\mathrm{eV}$ reproduces the experimentally obtained reaction yields as can be seen from Table 4.1, since $\nu_{\mathrm{TDS}} \approx \nu_{\mathrm{mod}}^{\mathrm{RW}}$ for this scenario.

This means that modeling of scenario C, which considers a barrier height of $E_{\mathrm{a}} = 1.0\,\mathrm{eV}$, underestimates the measured reaction yields by at least four orders of magnitude. Thus, only

qualitative (fluence dependence and 2PC lineshape) but no *quantitative* (yields) agreement between experiment and model is achieved with scenario C.

In summary, one can state that only scenario A is capable of reproducing the experimental data *qualitatively* and *quantitatively* in agreement with the TDS data and the calculated DFT activation energy of 1.8 eV [And05]. This means that non-adiabatic adsorbate-substrate coupling has to be considered in the fs-laser induced associative desorption of CO from Ru(001).

Isotope effect

As explained in Section 1.3.3, an isotope effect concerning desorption yields should be observed, with higher yields for the lighter isotope. Experimentally, no isotope effect is found as shown in Section 4.2.4. The isotope effect can be modeled by using mass-dependent electronic friction coefficients according to Eq. (1.45). Since the barrier towards reaction is mainly along the intramolecular distance d, the reduced mass μ of the CO molecule has to be taken into account. Applying the experimental parameters given in Section 4.2.4, an modeled isotope effect of

$$\frac{Y(^{13}\mathrm{C}^{16}\mathrm{O})}{Y(^{13}\mathrm{C}^{18}\mathrm{O})} \approx \frac{Y(^{12}\mathrm{C}^{18}\mathrm{O})}{Y(^{13}\mathrm{C}^{18}\mathrm{O})} = 1.08. \tag{4.14}$$

results for the electron and phonon driven reaction. This is within the uncertainties of the experimental data which exhibit yield ratios of 1.05(6) and 0.97(6) for isotopic substitution of O and C, respectively. Thus, a non-observed isotope effect is in accordance with a non-adiabatic reaction mechanism, where the barrier is located along the intramolecular coordinate.

Transient adsorbate temperature and reaction rate

The calculated transient adsorbate temperatures $T_{\mathrm{ads}}(t)$ and reaction rate $R(t)$ corresponding to an electron and phonon mediated reaction scenario are depicted in Fig. 4.14. In addition,

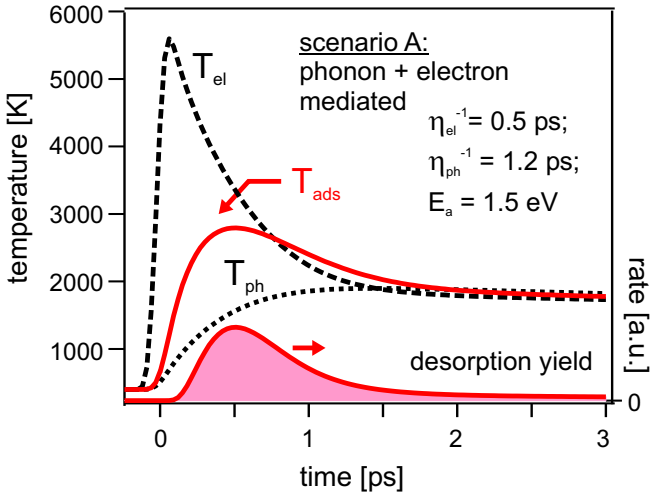

Figure 4.14.: Temperature transients of the coupled heat baths and the resulting desorption rate calculated for scenario A. Coupling to the electrons and the phonons is taken into account via $\eta_{\mathrm{el}}^{-1} = 0.5\,\mathrm{ps}$ and $\eta_{\mathrm{ph}}^{-1} = 1.2\,\mathrm{ps}$. An activation energy of $E_{\mathrm{a}} = 1.5\,\mathrm{eV}$ is considered. The underlying experimental conditions correspond to the 2PC experiment at zero delay.

the temperature transients T_{el} and T_{ph} of the electron and phonon heat bath after fs-laser excitation at $t = 0$ are given. $T_{\mathrm{ads}}(t)$ follows mainly the electron temperature T_{el} and peaks after $t = 0.5\,\mathrm{ps}$, when also $R(t)$ exhibits the maximum. No significant reaction rate is obtained for times larger than 2 ps which means that the reaction occurs on an ultrafast timescale $\leq 2\,\mathrm{ps}$.

4.4. Discussion

Although no direct experimental evidence was found for non-adiabatic adsorbate-substrate coupling contributing to the fs-laser induced associative desorption of CO from Ru(001), modeling of the data within the framework of a frictional approach revealed that a purely phonon mediated scenario is not capable of reproducing the experimental findings. In the following, the strength of the determined non-adiabatic coupling and the implications of using a 1D model for a multi-dimensional problem will be discussed. Furthermore, the measured translational energies of the desorbing CO molecules will be related to the dimensionality and the kinetics of the investigated surface reaction.

Non-adiabatic coupling strength

The non-adiabatic coupling is determined by modeling the experimental data. $\eta_{\mathrm{el}} = 2 \cdot 10^{12}\,\mathrm{s}^{-1}$ corresponding to an ultrafast coupling time of $\eta_{\mathrm{el}}^{-1} = \tau_{\mathrm{el}} = 500\,\mathrm{fs}$ is obtained. This coupling time is of the same order of magnitude as those found for the H(D)/Ru(001) system [Den03b, Den04] (see also Section 3.1.2). This means that the almost one order of magnitude heavier atoms C and O with respect to H(D) are accelerated on the same timescale which thus requires one magnitude larger mass-independent friction coefficients γ_{el} (see Eq. (1.45)). As mentioned in Section 4.1.1, Luntz and Persson [Lun05] calculated mass-independent *ab initio* electronic friction coefficients γ_{el} for the isoelectronic N_2/Ru(001) system, which is believed to be comparable to the present system due to the similarities of the underlying PESs [Mav99, Ham00b]. To compare γ_{el} with the fit parameter η_{el} the mass-weighted average of the two components along the intramolecular distance d and the distance z between surface and center-of-mass is obtained by

$$\langle \eta_{\mathrm{el}} \rangle \approx \frac{1}{2} \left(\frac{\langle \gamma_{dd} \rangle}{\mu} + \frac{\langle \gamma_{zz} \rangle}{m} \right), \tag{4.15}$$

where μ and m denote the relative mass and absolute mass of the molecule, respectively. γ_{dd} and γ_{zz} closest to the minimum of the PES energy are considered, since γ increases towards the transition state. A inverse frictional coupling time of $1/560\,\mathrm{fs}^{-1}$ is obtained for N_2/Ru(001) and in very good agreement with the value found for the CO recombination. This implies that a coupling strength one order of magnitude larger than for the H/Ru(001) system is reasonable for the present case and can be rationalized considering that the formation of π-bonds on metal surfaces requires strong mixing between molecular states and metal bands [Lun05].

Dimensionality considerations

It is astonishing that a one-dimensional (1D) model is capable of reproducing the experimental data so well, since the associative CO desorption is at least a six-dimensional (6D) problem. For the fs-laser induced electron mediated associative desorption of hydrogen from Ru(001) discussed in Chapter 3, the 1D friction model is also applied successfully [Den03b, Den04, Wag05]. Two-dimensional (2D) molecular dynamic calculations including *ab initio* electronic

frictional coupling[6] performed by Luntz et al. [Lun06] for this system revealed that the success of the 1D model is based on rapid interchange between the molecular coordinates during desorption. An analysis of the calculated trajectories[7] shows that not only the overall amount of energy transferred to the adsorbate determines the reaction rate, but also which molecular degree of freedom is excited. Excitation of the "wrong" degree of freedom does not lead to desorption even if the overall energy is large enough. It is shown that these phase space constraints can be considered in a 1D model in terms of an additional barrier leading to higher activation energies E_a than determined in TDS experiments, where the different degrees of freedom are thermally equilibrated. An increased barrier height by a factor of 1.5 compared to the TDS-value is indeed required to model successfully the results for the fs-laser induced associative desorption of hydrogen from Ru(001) with the 1D friction model [Den03b].

In the present investigation the fs-laser induced and the thermal desorption data are consistently described with the same activation energy E_a, which seems to be contradictory to the above argumentation. This paradox can be solved if one compares the topologies of the PESs governing the desorption processes. For the case of hydrogen and Ru(001), no pronounced barrier is existent[8] [Lun06] along the minimum reaction path which has to be "climbed" till the end for successful desorption. Thus, the adsorbate has to curve around the "elbow" of the PES, which is at least a 2D problem. For the case of CO and Ru(001) a high barrier is existent and mainly along the vibrational coordinate [Mav98]. Thus it could be that for successful desorption mainly a 1D "ascent" to the transition state is required and that the multi-dimensionality comes into play beyond this point of no return. This might explain why a 1D model reproduces successfully the experimental data without taken into account phase space constraints resulting in a higher 1D activation energy. However, this interpretation remains speculative until multidimensional dynamic calculations offer the possibility of investigating the desorption trajectories.

Mean translational energy

Multi-dimensionality comes also into play investigating the energy transfer into the different degrees of freedom of the nascent molecule during desorption. Figure 4.15 shows the mean translational energies $\langle E_{trans} \rangle$ for CO molecules desorbing normal to the surface. $T_{trans} = \langle E_{trans} \rangle / 2k_B$ is depicted as a function of the absorbed laser fluence $\langle F \rangle$ for the two data sets presented in Section 4.2.5. A moderate increase in T_{trans} with $\langle F \rangle$ is observed. In addition to the experimental data, a rate-weighted adsorbate temperature T_{ads}^{RW} for the electron and phonon mediated process, respectively, is plotted as a function of $\langle F \rangle$ in Fig. 4.15. The general trend of the experimental data is well described. Considering desorption of an adsorbate in thermal equilibrium with the surface at temperature T_S, an average translational energy of $\langle E_{trans} \rangle = 2k_B T_S$ is expected. This is not the case as can be seen by the factor 3 higher values for T_{ads}^{RW}.

In the case of the fs-laser induced hydrogen recombination already mentioned above, T_{ads}^{RW} was a factor of 1.4 lower than the measured T_{trans} [Wag05]. Luntz et al. showed that this effect is due to a small barrier (≈ 60 meV) along the translational coordinate z whose potential

[6] see Appendix A for details
[7] A more detailed discussion is given in Section 3.4.
[8] As can be seen in Section 3.1.1, Fig. 3.1.

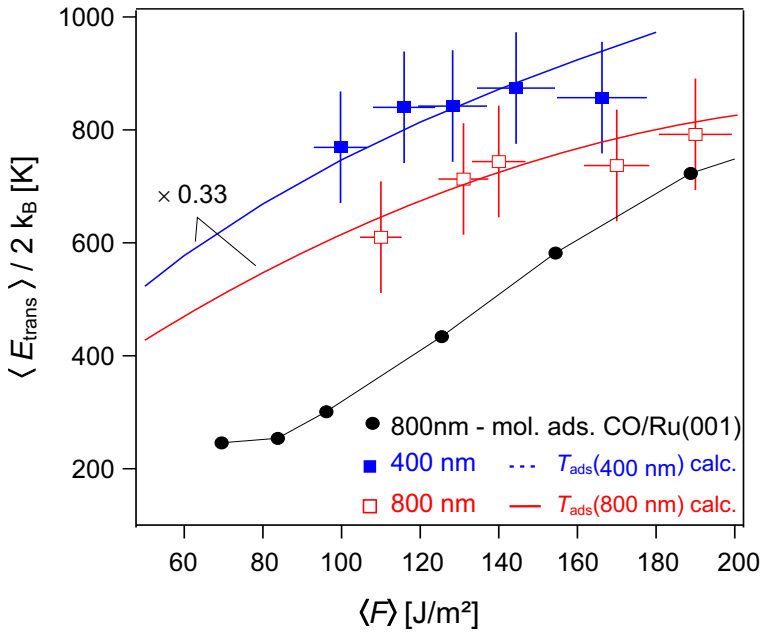

Figure 4.15.: Mean translational energies $\langle E \rangle = 2k_B T_{trans}$ of CO desorbing after fs-laser irradiation of an adsorbate covered Ru(001) surface as a function of absorbed laser fluence $\langle F \rangle$. Open and filled squares indicate associatively desorbing CO for same experimental conditions as in Section 4.2.2. Lines represent the calculated rate-weighted adsorbate temperatures T_{ads}^{RW}. Note the rescaling by a factor of 0.33.
Filled circles connected by a line as guide to the eye denote the translational temperatures of CO desorbing from a saturation covered Ru(001) surface ($T_S = 100$ K) of molecularly bound CO after irradiation with 800 nm fs-laser pulses (data taken from [Fun00]).

energy is released into the translation during desorption. In addition, the internal energy of the desorbing hydrogen molecules was investigated and a vibrational temperature T_{vib} a factor 1.5 lower than T_{ads}^{RW} has been observed[9]. Thus, one can expect a reversed scenario for the CO recombination, where due to the barrier location along the vibrational coordinate an enhancement of T_{vib} with respect to T_{trans} should be very likely. Knowledge about the energy transfer to the internal degrees of freedom of the desorbing CO is required before one can judge, if T_{ads}^{RW} is suited to describe the energy transfer to the desorbing molecules in terms of an energy balance as discussed in Section 3.3.

For the case of *thermal*, i.e. $T_{ads} \approx T_{el} \approx T_{ph}$, associative desorption of N_2 from Ru(001) such an energy balance breaks down. Diekhöner et al. measured the energy transfer to the internal molecular degrees of freedom of the desorbing N_2 and did not observe an enhanced T_{vib}, which is expected because of the high vibrational barrier [Die02]. Non-adiabatic coupling was considered via *ab initio* molecular dynamic calculations (see Appendix A) by Luntz and Persson [Lun05], which revealed that significant energy transfer to the substrate electrons has indeed to be considered in this system. The N_2/Ru(001) experiments indicate that there is non-adiabatic frictional coupling from the barrier to the gas phase N_2. No information is obtained about how the barrier is climbed, whereas in the fs-laser induced CO recombination, non-adiabatic coupling has to be considered on the "atomic side" of the transition state. Thus, one has to be careful by comparing the outcome of the two experiments directly, even though it

[9] This very brief characterization of the energy balance determined for the fs-laser induced hydrogen recombination on Ru(001) is subject of Chapter 3, where a very detailed description can be found.

is very likely that electronic damping is also relevant for the "molecular side" of the transition state in the associative CO desorption process.

Furthermore, one has to consider that $T_{\mathrm{ads}}^{\mathrm{RW}}$ represents only the activation step of the desorption process and thus, is not necessarily suited to describe the "descent" from the barrier. Accordingly, the calculated reaction rate $R(t)$ must not be understood as the desorption time, which strongly depends on the molecular trajectories and thus on the topology of the PES. For CO/O/Ru(001) a deep molecular well of $\approx 1\,\mathrm{eV}$ exists, to which CO is bound in an upright configuration [Hof91, Kos92]. Thus it is very likely that the CO is either transiently trapped into or indirectly scattered from the molecular well after association at the barrier and before exiting into the gas phase, which involves an erection of the molecule. This means that the CO looses its "memory" about the activation step in or at the chemisorption well.

This scenario is supported by experiments performed by Diekhöner and coworkers [Die01] who investigated the thermal associative desorption of CO from Ru(001). Despite the thermal activation of the reaction, similar translational energies of the desorbing CO have been determined as for the fs-laser induced reaction. This corroborates the idea of a scenario where the CO loses its memory about its formation in the chemisorption well before it desorbs.

Full thermal accommodation with the substrate is not observed as can be seen from a comparison of the modeled phonon temperature $T_{\mathrm{ph}} \approx 1500\,K$ (see Fig. 4.14) and $T_{\mathrm{trans}} \approx 800\,\mathrm{K}$. This behavior was also observed by Funk and coworkers [Fun00] who investigated the fs-laser induced desorption of *molecularly* bound CO from Ru(001). The translational temperatures for CO desorbing from the chemisorption well of a saturation covered Ru(001) surface with initial temperature $T_{\mathrm{S}} = 100\,\mathrm{K}$ is also depicted in Fig. 4.15. A phonon mediated desorption process was determined and $T_{\mathrm{ads}}^{\mathrm{RW}}$ was also found to be a factor 2 to 3 higher than T_{trans} [Fun00]. This behavior was contributed to dynamical cooling elaborated theoretically by Tully [Tul81] for the adsorption and desorption of rare gas atoms at a platinum surface. Since the PES is significantly different for a strongly chemisorbed adsorbate like CO and rare gas atoms, it is questionable if the consideration of dynamical cooling is appropriate for the CO/Ru(001) system. Dynamical cooling originates from insufficient energy transfer between adsorbate and substrate during interaction [Tul81]. This means that systems exhibiting dynamical cooling should also exhibit a significant decrease of the sticking probability of impinging particles with increasing particle energy since not enough energy can be dissipated to the substrate during interaction. This is not observed for CO/Ru(001) where the initial sticking coefficient only trivially falls off from 1.0 to 0.6 for kinetic energies of the impinging molecule ranging from 0.09 to 2.0 eV [Kne99]. Therefore by detailed balance, there has only negligible cooling to be considered in desorption of CO from Ru(001).

The differences in T_{trans} for the three data sets depicted in Fig. 4.15 are easily explained by the different experimental parameters. The slightly higher translational temperatures measured for CO desorbing after excitation with 400 nm fs-laser pulses are consistent with the higher surface temperatures resulting from the shorter optical penetration depth of the laser pulse (see above). The larger differences between the two data sets obtained from excitation with 800 nm fs-laser pulses can be contributed to the different initial surface temperatures of 100 and 400 K, whereby the higher temperature corresponds to the recombinative desorption.

The considerations discussed above imply that the outcome of the two-temperature model, namely the calculated surface temperatures are correct. Lisowski and et al. investigated the ultrafast dynamics of electron thermalization, cooling and transport effects in Ru(001)

(T_S = 100 K) after fs-laser excitation. They show that the 2TM overestimates the phonon temperature T_{ph} by a factor 2 under their experimental conditions. They can achieve quantitative agreement with the experimental data, if ultrafast energy transport by ballistic electrons is incorporated in the model. The efficiency of the ballistic transport depends strongly on the mean free path of the electrons, which decreases with increasing phonon temperature due to an increase of the electron-phonon scattering rate. At 100 K, the mean free path for electrons is $\approx$ 20 nm, whereas a factor 10 shorter mean free path is found at 400 K [Bas82]. This means that the influence of energy transport away from the surface by ballistic electrons should only be a minor correction to the 2TM for surface temperatures present in the CO recombination process, whereas the data for CO desorbing directly from the molecular bound state with an initial surface temperature T_{ads} have to be considered with some caution.

Summarizing, the observed low translational temperatures T_{trans} of the CO molecules desorbing associatively from Ru(001) can not be assigned to a distinct physical origin as long as the energy transfer to the internal molecular degrees of freedom is unknown. Frictional damping during desorption or unequal energy partitioning into the different degrees of freedom or dynamical cooling are plausible scenarios to explain the experimental findings, whereas dynamical cooling and inadequately calculated phonon temperatures are excluded.

4.5. Summary and Outlook

Summarizing, it has been shown that the fs-laser induced associative desorption of CO from Ru(001) under the present experimental conditions is a first order process. *Qualitative* and *quantitative* successful modeling of the experimental data requires to take into account an one order of magnitude larger mass-independent electronic coupling strength than for the H_2/Ru(001) system. This is consistent with theoretical predictions for the related system N_2/Ru(001).

As can be seen from the modeled reaction rates, the barrier towards desorption is overcome within ≈ 1 ps after excitation so that the fs-laser induced CO recombination has to be considered as an ultrafast surface reaction. This means that an experimentally determined 2PC width of ≈ 20 ps must not automatically be interpreted as an indication for a slow, purely phonon mediated reaction.

The observed wavelength dependence of the reaction yield is rationalized in terms of wavelength dependent optical penetration depths and is not due to non-thermal electrons which might in principle enhance a surface reaction governed by a higher-lying unoccupied adsorbate resonance. Such a diabatic scenario would also be inconsistent with the success of the applied friction model in the low friction limit and constant frictional coupling. The capability of a one-dimensional model to describe a multi-dimensional reaction, can be understood in terms of the reduced dimensionality of the activation step initiating the desorption process.

The discussion of the determined low translational energies of the desorbing CO flux remains speculative as long as the energy transfer to the internal molecular degrees is unknown. Two scenarios, either dynamical cooling or unequal energy partitioning into the different degrees of freedom have been discussed and seem to be plausible.

Additional information, especially about the timescales on which the associative CO desorption takes place is in principle accessible from time-resolved investigations of the reaction. A possible experimental approach is illustrated in Fig. 4.16. In such a pump-probe scheme, the

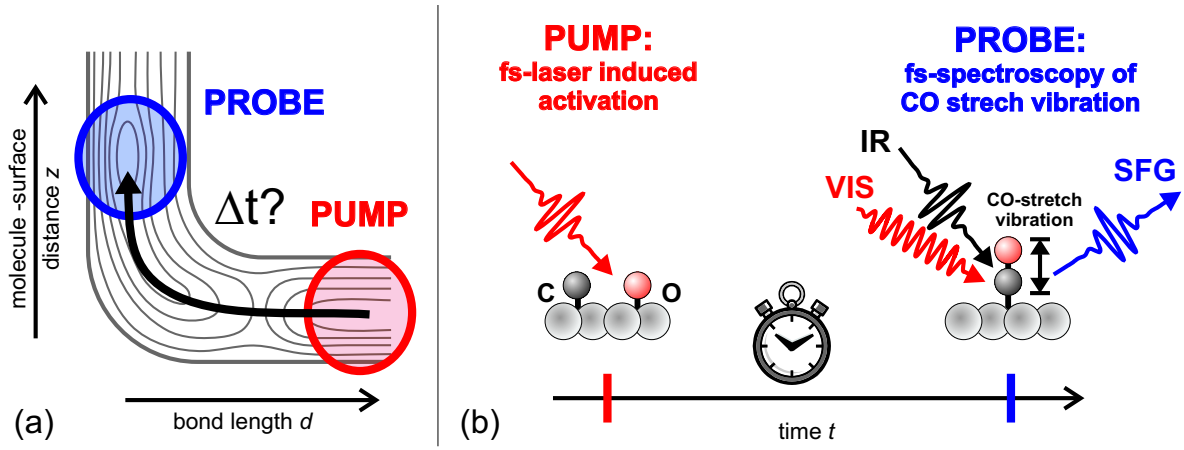

Figure 4.16.: Illustration of a PUMP-PROBE experiment for determining the reaction dynamics directly. (a) The reaction is initiated by a first PUMP pulse and a delayed PROBE pulse determines the population of molecular CO in the chemisorption well at a certain time delay Δt. (b) The formation of molecular CO is evidenced by probing the internal CO stretch vibration time-resolved via resonant fs-IR-VIS-SFG.

time delay Δt between two laser pulses can be varied and the earlier pump pulse initiates the reaction, whereas the later probes a specific quantity of the system under investigation. In the illustration, this quantity is the intramolecular CO stretch vibration, which is only existent after the molecule is formed and thus specific for a successful traverse of the activation barrier. Time-resolved vibrational spectroscopy via sum-frequency generation as explained in Section 2.4.4 would therefore be a suited method to measure the transient CO stretch vibration after fs-laser excitation of the O/C/Ru(001). The appearance of the CO stretch vibration could then by directly related to the time it takes to form the molecule, i.e. the binding at the molecular chemisorption well, and the disappearance of the signal to the time, when the desorption out of the well took place.

Such an experiment was performed, but unfortunately, the transient CO-SFG signal was not detectable with the present experimental setup. An estimation of the required SFG data acquisition time is given in Appendix B and shows that approximately one week of data acquisition is required to measure one single pump-probe delay.